



Inhibition of sphingosine kinase 2 down-regulates ERK/c-Myc pathway and reduces cell proliferation in human epithelial ovarian cancer

Lan Dai^{1,2}, Wenjing Wang^{1,2}, Yixuan Liu^{1,2}, Keqi Song^{1,2}, Wen Di^{1,2,3}

¹Department of Obstetrics and Gynecology, Ren Ji Hospital, School of Medicine, Shanghai Jiao Tong University, Shanghai, China; ²Shanghai Key Laboratory of Gynecologic Oncology, Ren Ji Hospital, School of Medicine, Shanghai Jiao Tong University, Shanghai, China; ³State Key Laboratory of Oncogene and Related Genes, Shanghai Cancer Institute, Ren Ji Hospital, School of Medicine, Shanghai Jiao Tong University, Shanghai, China

Contributions: (I) Conception and design: W Di, L Dai, K Song; (II) Administrative support: W Di, L Dai; (III) Provision of study materials or patients: K Song, W Wang, Y Liu; (IV) Collection and assembly of data: L Dai, K Song, W Wang, Y Liu; (V) Data analysis and interpretation: L Dai, K Song, W Wang, Y Liu; (VI) Manuscript writing: All authors; (VII) Final approval of manuscript: All authors.

Correspondence to: Wen Di; Lan Dai; Keqi Song. Department of Obstetrics and Gynecology, Ren Ji Hospital, School of Medicine, Shanghai Jiao Tong University, Shanghai 200127, China. Email: diwen163@163.com; delta496@163.com; songkeqi@163.com.

Background: Epithelial ovarian cancer (EOC) is the leading cause of death from female cancers. In our previous study, sphingosine kinase 2 (SphK2) inhibitor was shown to display anti-EOC activities. The purpose of this study was to evaluate further the expression characteristics and clinical significance of SphK2 in EOC and to explore the roles and underlying mechanisms of SphK2 in EOC cell survival.

Methods: The expression of SphK2 was examined by immunohistochemistry (IHC) and Western blot, and its clinical implications and prognostic significance were analyzed. We performed a cellular proliferation assay, and a mouse xenograft model was established to confirm the roles of SphK2 *in vitro* and *in vivo*. Cell cycle analysis, apoptosis assay, and Western blot were performed to examine cell cycle progression and apoptosis rate. Gene set enrichment analysis (GSEA), and Western blot were used to investigate the downstream signaling pathways related to SphK2 function.

Results: The expression level of SphK2 was shown to be associated with stage, histological grade, lymph node metastasis, and ascites status. More importantly, a high SphK2 expression level was a prognostic indicator of overall survival (OS) and relapse-free survival (RFS). Moreover, knockdown of SphK2 arrested cell cycle progression and inhibited EOC cell proliferation both *in vitro* and *in vivo*. Furthermore, ERK/c-Myc, the key pathway in EOC progression, was important for SphK2-mediated mitogenic action in EOC cells.

Conclusions: Our findings provided the first evidence that SphK2 played a crucial role in EOC proliferation by regulating the ERK/c-Myc pathway. This indicated that SphK2 might serve as a prognostic marker and potential therapeutic target in EOC.

Keywords: Epithelial ovarian cancer (EOC); sphingosine kinase 2 (SphK2); extracellular signal-regulated kinase (ERK); c-Myc; proliferation

Submitted Oct 04, 2020. Accepted for publication Jan 17, 2021.

doi: 10.21037/atm-20-6742

View this article at: <http://dx.doi.org/10.21037/atm-20-6742>

Introduction

Epithelial ovarian cancer (EOC), the most lethal gynecologic malignancy, is the leading cause of death from female cancers (1). The majority of EOC patients are first diagnosed at late stages because the early-stage disease is virtually asymptomatic, which causes significantly poor prognosis and high mortality (2). Surgery combined with platinum/taxane chemotherapy represents the first-line treatment for EOC. Unfortunately, most patients, who initially respond to this treatment, eventually develop chemoresistance (3). Thus, the development of a novel therapeutic strategy is needed. Unlike traditional cytotoxic chemotherapy, targeted therapy inhibits cancer growth by interfering with specific molecules needed for cancer progression, which may become a new hope for EOC therapy (4,5). Understanding the underlining molecular mechanisms associated with EOC progression is therefore critical to identify new targets for new targeted therapy.

The roles of sphingolipids in cell biology and cell fate have been explored for several decades. There is accumulating evidence demonstrating that disturbed sphingolipid metabolism may contribute to cancer initiation and progression and present an exploitable target for cancer therapy (6). Sphingosine kinases (SphKs), ceramide, sphingosine, transmembrane transporters, sphingosine-1-phosphate (S1P), and S1P receptors (S1PRs) are the key players in the sphingolipid metabolic pathway. The “inside-out” model is widely used to explain the function of SphK/S1P/S1PR signaling (7). It is proposed that S1P, generated by SphK, can be secreted into the extracellular milieu and then activates S1PRs through autocrine and paracrine manners, leading to the activation of downstream signals. Moreover, S1P can also function intracellularly independent of S1PRs (8). Among the key players of the sphingolipid metabolic pathway, much attention has been paid to SphKs because their catalytic activity lies at the critical juncture in regulating sphingolipid metabolism. The SphKs exhibit 2 isoforms, SphK1 and SphK2, of which SphK1 has emerged as an important and critical signaling enzyme because it is involved in many aspects of cancer progression, such as proliferation, angiogenesis, metastasis, and chemoresistance (9-11). Consistent with this, we found previously that the expression level of SphK1 was significantly increased in EOC tissues and was associated with EOC metastasis and angiogenesis (12,13). Although the two isoforms of SphKs (SphK1 and SphK2) share high sequence similarity, they differ significantly in distribution, regulation, and function.

The role of SphK2 in cell survival is controversial, and both pro-apoptotic and pro-proliferative functions have been suggested. Initially, SphK2 was recognized as a pro-apoptotic protein because SphK2 over-expression inhibited the growth and promoted cancer cells' apoptosis (14,15). However, it was subsequently found to be pro-survival as SphK2 down-regulation or inhibition suppressed tumor cells' growth (16-18). Recent work has suggested that SphK2 plays a role in promoting cancer by regulating several important pro-oncogenic pathways, such as protein kinase B (AKT), extracellular signal-regulated kinase (ERK), and signal transducer and activator of transcription-3 (STAT3) pathways (19,20). Moreover, SphK2 could also work as an epigenetic regulator. For example, SphK2 was reported to enhance MYC expression, an important oncogene, via regulation of histone deacetylase 1/2 (HDAC1/2) (21). Until now, much is still unknown or controversial about SphK2.

Our research group recently found that treatment with an orally active and specific SphK2 inhibitor, ABC294640, significantly inhibited EOC cell proliferation and increased apoptosis (22). This result suggested SphK2 might be a potential target for EOC therapy. However, there is no available data on SphK2 expression patterns in EOC tissues and their clinical significance. Moreover, the molecular mechanisms of SphK2 in EOC growth remain largely unknown. This study aimed to evaluate the expression characteristics and clinical significance of SphK2 in EOC and explore the roles and underlying mechanisms of SphK2 in EOC cell survival through both *in vitro* and *in vivo* studies.

We present the following article in accordance with the ARRIVE reporting checklist (available at <http://dx.doi.org/10.21037/atm-20-6742>).

Methods

Reagents and antibodies

Antibodies against SphK2 (Abcam, ab264042, rabbit), c-Myc (Abcam, ab32072, rabbit), and glyceraldehyde 3-phosphate dehydrogenase (GAPDH) (Abcam, ab8245, mouse) were purchased from Abcam (Cambridge, MA, USA). Antibodies against ERK1/2 (CST, 4696, rabbit), phospho-ERK1 (Thr202/Tyr204)/ERK2 (Thr185/Tyr187) (CST, 4370, rabbit), cyclin D1 (CST, 2978, rabbit), phospho-Rb (CST, 8516, rabbit) were purchased from Cell Signaling Technology (Danvers, MA, USA). The inhibitor U0126 (Sigma, 662005) was ordered from Sigma-Aldrich (St. Louis, MO, USA).

Tissue specimens

Tissue specimens were collected from the patients without preoperative chemotherapy, including 5 normal ovarian tissues and 50 primary epithelial ovarian cancer (PEOC) tissues (stages I–II 20 cases, stages III–IV 30 cases). All procedures performed in this study involving human participants followed the Declaration of Helsinki (as revised in 2013). The institutional ethical committee approved this study of Renji Hospital (RA-2019-076), and all the participants provided informed consent.

Cell lines and culture conditions

Human EOC cell lines SKOV3 and OVCAR3 were obtained from American Type Culture Collection (ATCC). The SKOV3 cell line was routinely cultured in Dulbecco's Modified Eagle Medium (DMEM) (12430054, Invitrogen, Carlsbad, CA, USA) supplemented with 10% fetal bovine serum (FBS, Invitrogen, 16140071) and 1% antibiotics. The OVCAR3 cell line was routinely cultured in Roswell Park Memorial Institute-1640 (RPMI-1640) medium (Invitrogen, A1049101) supplemented with 20% FBS, 0.01 mg/mL insulin (Sigma-Aldrich, I0908), and 1% antibiotics. The A2780 was purchased from the China Center for Type Culture Collection (CCTCC) and routinely cultured in DMEM supplemented with 10% FBS and 1% antibiotics. The immortalized ovarian surface epithelial (IOSE) cell line was a gift from Prof. MW-Y Chan (National Chung Cheng University, Taiwan) and cultured in DMEM supplemented with 10% FBS and 1% antibiotics.

Immunohistochemistry

Immunostaining was performed and scored as previously described (12). The primary antibody used was anti-SphK2 (1:100, Abcam). The immunostaining intensity was scored as follows: negative [0], weak [1], moderate [2], and strong [3]. The proportion of positively stained tumor cells was assessed as follows: no positive tumor cells [0], <25% [1], 26–50% [2], 50–75% [3], and >75% [4]. Staining index (SI) was calculated as staining intensity score \times proportion score. The protein expression level was considered to be high when the score was >3 and low when the score was \leq 3.

Western blot analysis

Western blotting was performed as previously described (23). Briefly, cells were harvested after the indicated treatments and lysed with radioimmunoprecipitation assay (RIPA) buffer

plus protease inhibitors. The protein was quantified and resolved by 8–10% sodium dodecyl sulfate-polyacrylamide gel electrophoresis (SDS-PAGE) and transferred to polyvinylidene fluoride (PVDF) membranes. The membranes were then incubated with appropriate antibodies according to the manufacturer's standard methods. Finally, the proteins were visualized using an enhanced chemiluminescence detection kit (32109; Pierce, Lambertville, MI, USA).

Transient [small interfering RNA (siRNA)] and stable [short hairpin RNA (shRNA)] transfection

The siRNAs specifically targeting human ERK1 (5'-CAUGAAGGCCCGAAACUACUU-3'), ERK2 (5'-GCGCUUCAGACAUGAGAACUU-3'), and the scrambled control siRNA (5'-AAUUCUCCGAACGUGUCACGU-3') were synthesized by GenePharma (Shanghai, China). The siRNA duplexes were transfected using Lipofectamine (Invitrogen) according to the manufacturer's protocol. The shRNA lentiviral packaging plasmid specifically targeting human SphK2 (5'-AACCUCAUCCAGACAGAACGA-3') and the non-targeting negative control plasmid (5'-AAUUCUCCGAACGUGUCACGU-3') were constructed by GenePharma. Cell lines were transduced with lentiviral vectors at a multiplicity of infection (MOI) = 5. To establish the cells stably down-regulating SphK2, transfected cells were selected by culturing in puromycin. Single colonies of stable transfectants were isolated and expanded. Several independent clones were used to complete the experiment to avoid errors caused by the clonal effect.

Real-time RT-PCR

The RNA was extracted by TRIzol Reagent (Thermo Fisher, Waltham, MA, USA). The messenger RNA (mRNA) levels were measured by Synergy Brands, Inc. (SYBR) Green reverse transcription polymerase chain reaction (RT-PCR) and then calculated by $2^{-\Delta\Delta Ct}$ method. Primers were as follows: SphK2, 5'-GGTTGCTTCTATTGGTCAATCC-3' (forward) and 5'-GTTCTGTCTGTTCTGTCTGGATG-3' (reverse); GAPDH, 5'-TGCACCACCAACTGCTTAGC-3' (forward) and 5'-GGCATGGACTGTGGTCATGAG-3' (reverse) (23).

Cellular proliferation assay

Cell proliferation was assessed using WST-1 (11644807001;

Roche, Basel, Switzerland) assay as previously described (24). Briefly, the indicated cells were seeded into 96-well plates, and the cell number was measured at 24, 48, 72, and 96 h. At each time point, WST-1 assay reagent was added into each well and cultured at 37 °C for 2 h. The supernatant from each well was then collected for measurement of absorbance at 450 nm. There was a direct correlation between the cell number and the absorbance at 450 nm in the current study.

Animal studies

All animal experiments were carried out following the National Institutes of Health (NIH) Guide for the Care and Use of Laboratory Animals 2018 and approved by Shanghai Jiao Tong University School of Medicine. The experimental protocols were approved by the Institutional Animal Care and Use Committee of Shanghai Jiao Tong University School of Medicine (A2018021). Mice were purchased from the Chinese Academy of Sciences. The mice were housed in a climate-controlled facility with free access to food and water. The animals' environment was a 12 h light/dark cycle with a constant temperature of 22±1 °C and humidity of 55%±5%. To establish subcutaneous transplantation models, female BALB/c nu/nu mice aged 5–6 weeks (8 mice in each group) were subcutaneously injected with 2×10⁶ EOC cells stably transfected with indicated plasmids. Tumor volumes were calculated twice a week using the following formula: $V = (\text{largest diameter} \times \text{small diameter} \times \text{depth}) \times \pi/6$. The mice were sacrificed 28 days after injection of EOC cells, and the weight of tumors was measured.

Cell cycle analysis

Cells were trypsinized, and 1×10⁶ cells were used for analysis. Cells were fixed in 70% ice-cold ethanol overnight and stained with propidium iodide at room temperature for 45 min. The cellular DNA content was analyzed by flow cytometry.

Apoptosis assay

Cells were harvested, and 1×10⁶ cells were used for analysis. The annexin V-FITC/PI apoptosis detection kit [556547; BD Biosciences, San Jose, CA, USA] was used to identify apoptotic cells by flow cytometry following the manufacturer's instructions.

Microarray analysis

Tumor RNA was prepared with RNeasy Plus Mini Kit (74134; Qiagen, Hilden, Germany) according to the manufacturer's protocol. Total RNA was subjected to microarray analysis with Whole Human Genome Oligo Microarray (Agilent, Santa Clara, CA, USA).

Statistical analysis

Statistical analyses were performed by using the SPSS software (IBM, Chicago, IL, USA). The χ^2 test was used to analyze the correlations between SphK2 expression and the clinicopathologic features of EOC (20,25). Kaplan-Meier curves and log-rank tests were used to analyze the survival data. Each experiment was performed independently in triplicate in our research. The values were presented as the mean ± standard deviation (SD) and were analyzed by *t*-test. A P value less than 0.05 was considered significant.

Results

SphK2 expression patterns in primary EOC tissues

The SphK2 protein expression was examined in 50 PEOC and 5 normal ovarian tissue specimens by immunohistochemical (IHC) staining. Representative photographs of SphK2 immunostaining are shown in *Figure 1A*. High SphK2 expression was shown in 62% [31/50] of the PEOC specimens and 38% [19/50] showed low expression. In contrast, none of the normal ovarian tissue specimens exhibited high SphK2 expression. As a negative control, normal rabbit immunoglobulins were substituted for primary antibodies (*Figure S1A*). The IHC staining of SphK2 in human breast cancer tissue, which is SphK2 positive, was used as a positive control (*Figure S1B*). Consistent with the findings from tissue specimens, the expression of SphK2 was significantly elevated in all 4 EOC cell lines examined compared to IOSE cells, an immortalized non-tumorigenic human ovarian surface epithelial cell line (*Figure 1B*). We further examined the relationship between SphK2 expression levels in PEOC and clinic-pathological characteristics (*Table 1*). High SphK2 expression level was associated with higher International Federation of Obstetrics and Gynecology (FIGO) stage ($P=0.001$), higher histological grade ($P=0.049$), lymph node metastasis ($P=0.001$), and ascites ($P=0.012$), which indicated that SphK2 expression was linked to the oncogenic behavior of EOC. However, we observed no correlation between SphK2 levels and age and histologic subtypes.

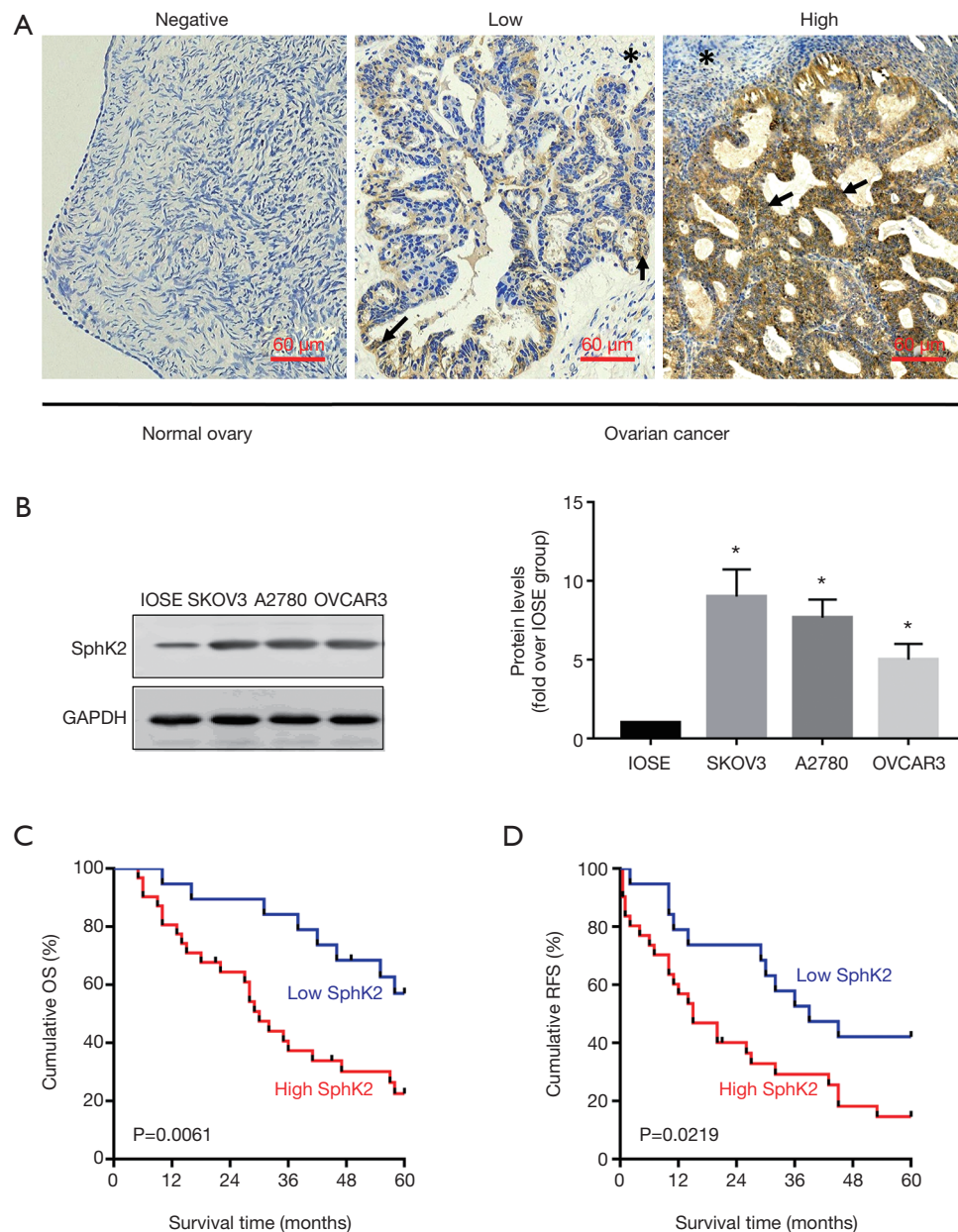


Figure 1 SphK2 over-expression in human ovarian cancer and its prognostic significance. (A) IHC staining of SphK2 in normal ovary and serous ovarian cancer tissues. The scale bar represents 60 μ m. Ovarian cancer tissue containing malignant cells, which are SphK2 positive (arrow), and SphK2 negative adjacent stroma (star). (B) Western blot analysis of SphK2 in IOSE cell line and ovarian cancer cell lines. (C,D) Kaplan-Meier curves showing OS and RFS of ovarian cancer patients. Curves show low (blue line, 19 cases of ovarian cancer patients) and high SphK2 protein expression (red line, 31 cases of ovarian cancer patients). The experiments were repeated 3 times. *, $P < 0.05$. SphK2, sphingosine kinase 2; IHC, immunohistochemical; IOSE, immortalized ovarian surface epithelial; OS, overall survival; RFS, relapse-free survival

Table 1 Clinicopathological features of ovarian tissue with regard to the relative expression of SphK2

Parameters	No. cases	SphK2 expression		χ^2	P value
		Low	High		
Age (years)				1.422	0.233
≤ Mean	21	10	11		
> Mean	29	9	20		
FIGO stage				10.314	0.001*
I-II	20	13	7		
III-IV	30	6	24		
Histologic grade				3.861	0.049*
I	7	5	2		
II-III	43	14	29		
Histology				5.675	0.059
Serous	42	13	29		
Mucinous	3	2	1		
Endometrioid	5	4	1		
Lymph node metastasis				11.297	0.001*
Absent	13	10	3		
Present	37	9	28		
Ascites				6.376	0.012*
Negative	18	11	7		
Positive	32	8	24		

*, P<0.05. SphK2, sphingosine kinase 2; FIGO, International Federation of Gynecology and Obstetrics.

Correlations between SphK2 expression level and survival analysis

The prognostic value of SphK2 was analyzed by comparing the overall survival (OS) and relapse-free survival (RFS) of patients with high and low SphK2 expression. Kaplan-Meier analysis showed that patients with high SphK2 expression had a significantly lower postoperative 5-year OS and a significantly lower postoperative RFS than those with low SphK2 expression (*Figure 1C,D*) (P<0.01). Together, these data suggested that SphK2 was a potentially useful predictor for the outcome of EOC.

SphK2 is required for EOC cell growth in vitro and in vivo

To assess the importance of SphK2 in EOC cells, we performed shRNA-based knockdown experiments in human EOC cell lines, which resulted in an efficient reduction in SphK2 mRNA

and protein levels compared to the control cells transfected with a negative control vector (*Figure 2A,B*). Proliferation assays revealed that SKOV3 cells subjected to SphK2 knockdown by shRNA were strongly inhibited in cell growth compared to controls (*Figure 2C*). To investigate whether SphK2 also has a role in EOC progression, we used a subcutaneous transplanted model of ovarian cancer in nude mice (8 mice in each group). The mice were subcutaneously injected with SphK2-downregulated SKOV3 cells or control cells, and tumor growth was measured after 1 month. As shown in *Figure 2D,E,F*, the SphK2-downregulated cell tumors were much smaller than the control cell tumors. Together, these results showed that SphK2 is critical for EOC cell growth *in vitro* and *in vivo*.

SphK2 controls cell cycle progression of EOC cells

To investigate the cellular mechanisms by which SphK2 was required for ovarian cancer cell growth, we used SKOV3 to

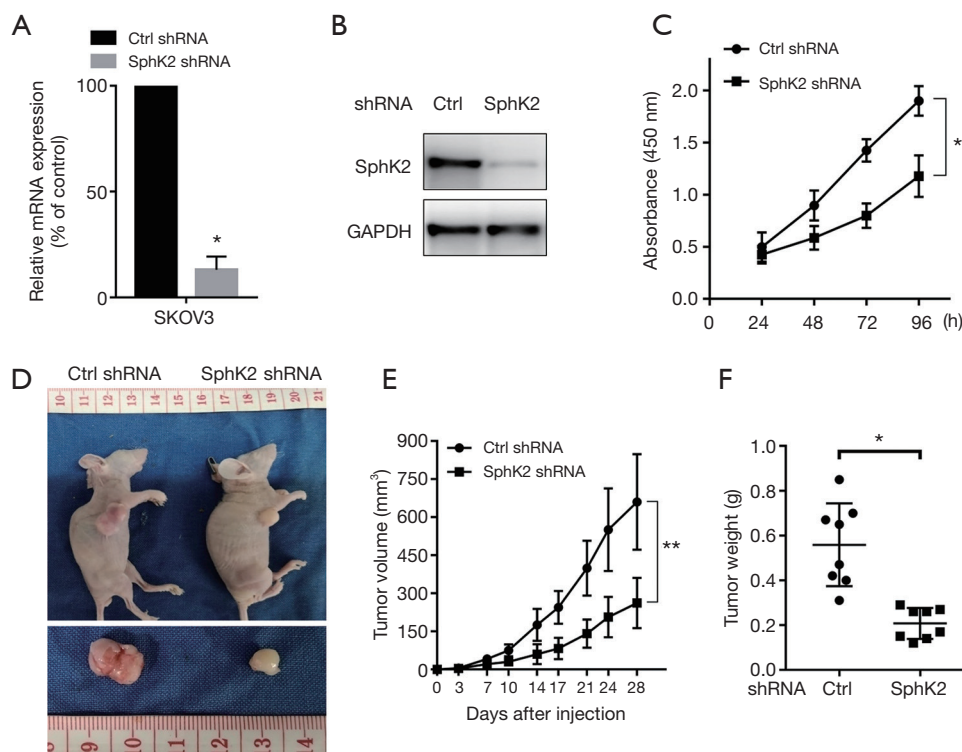


Figure 2 SphK2 inhibition suppresses the growth of EOC cells in vitro and in vivo. (A) SKOV3 cells transfected with control shRNA or SphK2 shRNA. Expression of SphK2 mRNA levels determined by PCR and normalized to GAPDH mRNA. (B) Protein levels of SphK2 as determined by Western blot. (C) A significant reduction in cell growth rate in the SphK2 shRNA group is observed by the cellular proliferation assay in ovarian cancer cells. (D) Representative images of tumors in subcutaneous ovarian cancer xenograft model. Mean tumor volume (E) and weight (F) in the SphK2 shRNA group are significantly reduced compared with the control group (8 mice in each group). The experiments were repeated 3 times. *, $P < 0.05$; **, $P < 0.01$. SphK2, sphingosine kinase 2; EOC, epithelial ovarian cancer; shRNA, short hairpin RNA; GAPDH, glyceraldehyde-3-phosphate dehydrogenase.

analyze the effects of SphK2 down-regulation on cell cycle and apoptosis. Compared to the control cells, shRNA-mediated SphK2 inhibition resulted in an accumulation of SKOV3 in the G0/G1 phase to reduce cells in the S phase (Figure 3A). Moreover, subsequent Western blot analysis indicated that SphK2 down-regulation reduced the levels of cyclin D1 and phosphor Rb (Figure 3B). In contrast to the strong effects on cell cycle progression, SphK2 down-regulation did not affect the apoptotic rate of ovarian cancer cells (Figure 3C). Together, these data suggested that SphK2 inhibition in ovarian cancer cells induces cell cycle G0/G1 arrest.

SphK2 inhibition in ovarian cancer cells induces an expression profile linked to the MAPK signaling pathway and MYC targets

To investigate the underlying molecular mechanisms

whereby SphK2 is required for EOC cell growth, we performed a microarray analysis of ovarian cancer SKOV3 cells transfected with shRNA targeting SphK2. Heatmap clustering of the top 100 upregulated or downregulated genes (Figure 4A, Table S1) showed a high degree of reproducibility between triplicates (26) and a significant differentiation between the SphK2 knockdown cells and the cells transfected with scramble control. Gene set enrichment analysis (GSEA) was used to analyze the SphK2-regulated gene signatures. The Kyoto Encyclopedia of Genes and Genomes (KEGG) pathway analysis revealed that genes deregulated upon SphK2 suppression were enriched for gene sets such as mitogen-activated protein kinase (MAPK) signaling pathway (Figure 4B,C). Consistent with the link to the MAPK pathway, GSEA analysis revealed significant associations with the gene set involving ERK/MAPK targets (Figure 4D). Intriguingly, the results of GSEA showed the

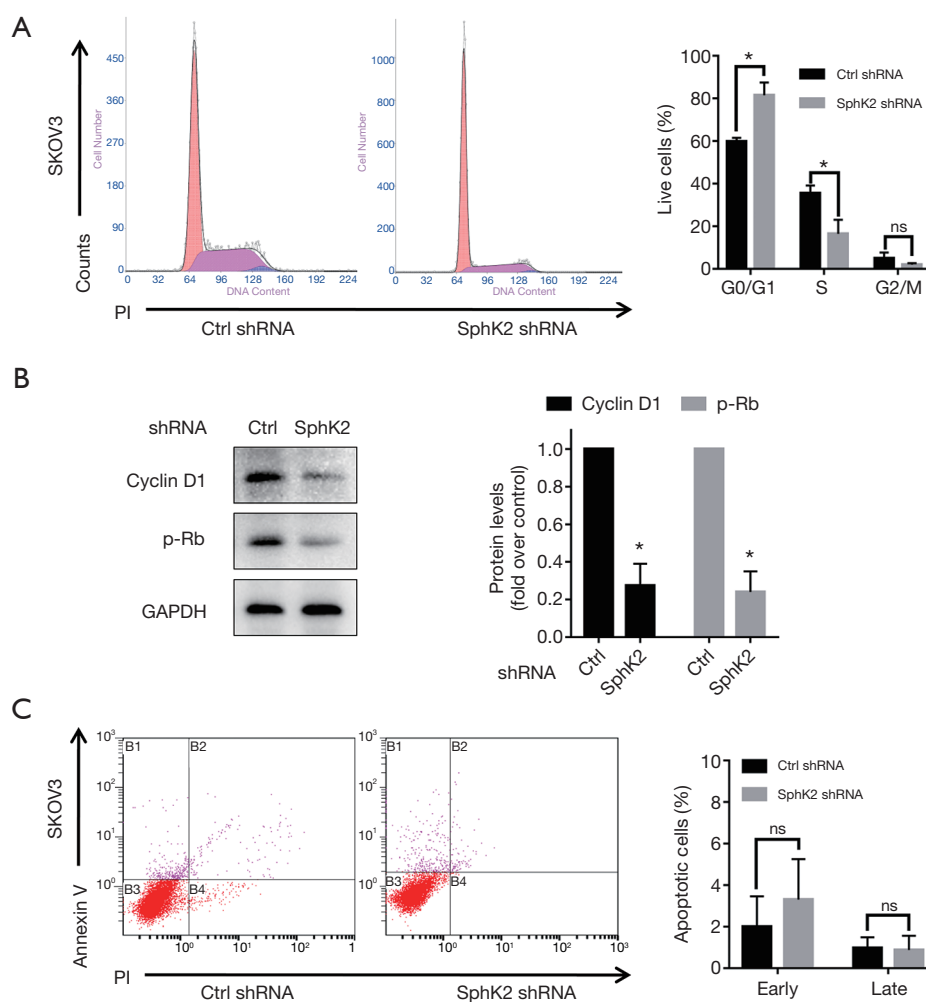


Figure 3 SphK2 inhibition in EOC cells causes an arrest in the G0/G1 phase of the cell cycle. (A) Representative flow cytometry charts of SKOV3 cells transfected with SphK2 shRNA or Ctrl shRNA and stained by PI. The percentage of cells in each cell cycle population was quantified. (B) Western blot analysis of cyclin D1 and p-Rb in ovarian cancer cells transfected with SphK2 shRNA or Ctrl shRNA. Right panels show that densitometric analysis of cyclin D1 and p-Rb (normalized to GAPDH) is reduced in SKOV3. (C) Bar graphs showing the percentage of apoptotic cells of SKOV3 transfected with SphK2 shRNA or Ctrl shRNA. The experiments were repeated 3 times. *, $P < 0.05$. SphK2, sphingosine kinase 2; EOC, epithelial ovarian cancer; Ctrl, control; shRNA, short hairpin RNA; PI, propidium iodide; p-Rb, phosphate retinoblastoma; GAPDH, glyceraldehyde-3-phosphate dehydrogenase.

expression changes in response to SphK2 inhibition were most significantly correlated with the gene signature of two individual subgroups of MYC targets data sets (Figure 4E,F, Tables S2,S3).

SphK2 down-regulation may induce c-Myc inhibition partly through the ERK1/2 pathway

The ERK1/2 pathway is one of the best-characterized members of the MAPK family. Moreover, it has been

demonstrated to play essential roles in cell cycle progression and cell survival (27). Thus, we detected the expression level of phosphorylated ERK1/2 protein by Western blot and confirmed that SphK2 inhibition down-regulated the ERK1/2 pathway activation (Figure 5A). The most widely studied gene in the MYC family, c-Myc, is involved in cell cycle regulation, cell proliferation, and differentiation (28,29). Down-regulation of c-Myc after SphK2 blockage was also confirmed by Western blot (Figure 5A). It has been reported that c-Myc is an inducible gene of ERK (30). To determine whether the down-regulation

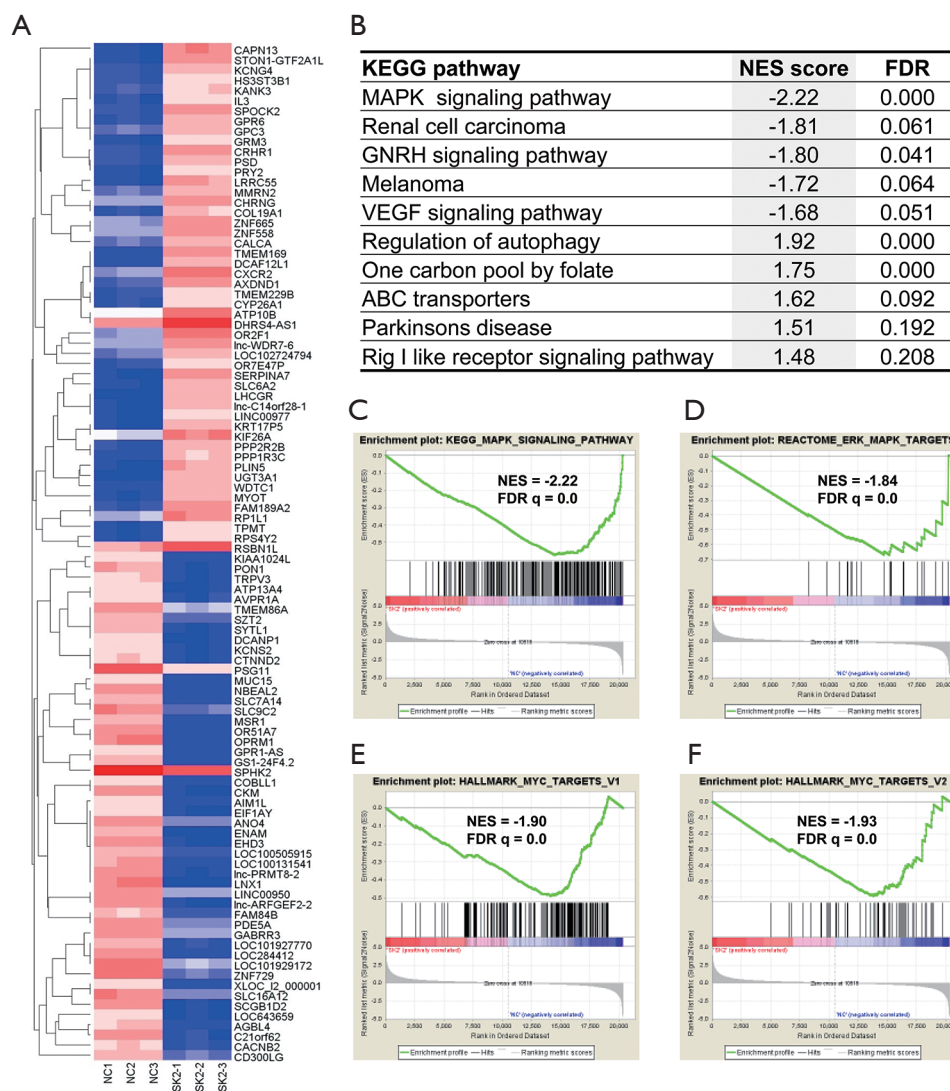


Figure 4 SphK2 suppression induces an expression profile correlating to MAPK signaling pathway and MYC targets. (A) Heatmap of 100 genes with most significant changes in gene expression of SKOV3 cells transfected with SphK2 shRNA or Ctrl shRNA. Blue and red colors represent low and high relative gene expression levels, respectively. (B) List of the ten most significant KEGG gene set pathways correlating to gene expression changes resulting from SphK2 knockdown in SKOV3 cells. (C,D,E,F) GSEA shows significant association between SphK2 level and several gene sets, including MAPK signaling pathway (C), ERK MAPK targets (D), MYC target V1 (E) and MYC target V2 (F). SphK2, sphingosine kinase 2; MAPK, mitogen-activated protein kinase; MYC, myelocytomatosis; shRNA, short hairpin RNA; KEGG, Kyoto Encyclopedia of Genes and Genomes; ERK, extracellular regulated protein kinases; GSEA, gene set enrichment analysis.

of c-Myc was partly through the ERK1/2 pathway in EOC cells, we investigated the effect of ERK1/2 blockage on c-Myc expression. As expected, ERK1/2 blockage by U0126, a specific inhibitor of the ERK1/2 pathway, significantly inhibited c-Myc expression (Figure 5B). Moreover, ERK1/2 knockdown also resulted in the suppression of c-Myc (Figure 5C). These results suggested that SphK2 down-regulation caused

c-Myc and ERK1/2 pathway inhibition. Knockdown of SPHK2 induced by ERK1/2 pathway suppression may contribute to the down-regulation of c-Myc.

Discussion

In the current study, we found that SphK2 played a crucial

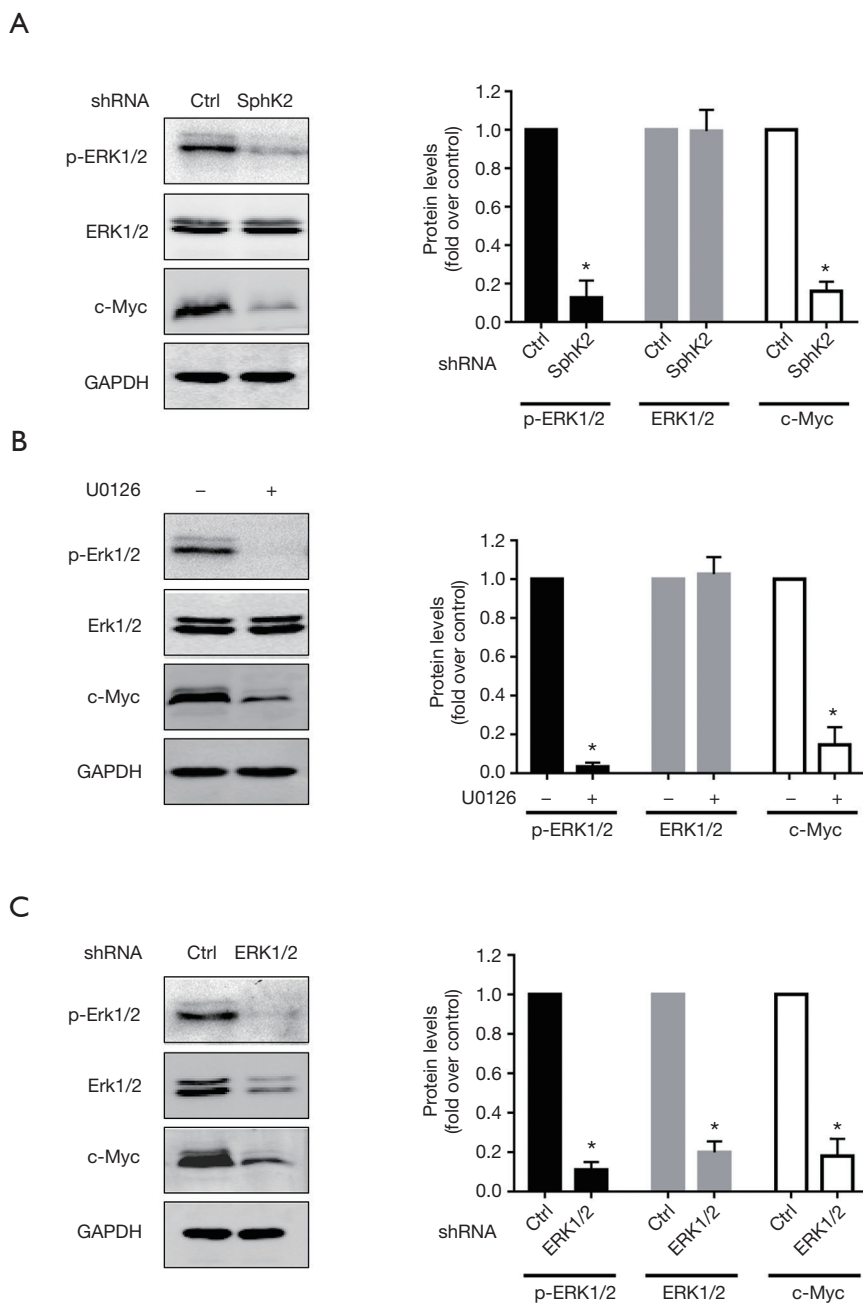


Figure 5 SphK2 blockage induces c-Myc inhibition partly through ERK1/2 pathway. (A) Western blot analysis of p-ERK1/2, ERK1/2, and c-Myc in ovarian cancer cells transfected with SphK2 shRNA or Ctrl shRNA. SphK2 inhibition reduces expressions of p-ERK1/2 and c-Myc not affecting ERK1/2. (B) Pretreatment with U0126, inhibitor of ERK1/2 pathway, also reduces the expressions of p-ERK and c-Myc in ovarian cancer cells. (C) Western blot analysis of p-ERK1/2, ERK1/2, and c-Myc in ovarian cancer cells transfected with ERK1/2 siRNA or Ctrl siRNA. Right panels show densitometric analysis of p-ERK1/2, ERK1/2, and c-Myc (normalized to GAPDH) corresponding to the bands shown in the Western blots. The experiments were repeated 3 times. *, $P < 0.05$. SphK2, sphingosine kinase 2; c-Myc, cellular myelocytomatosis; ERK, extracellular regulated protein kinases; shRNA, short hairpin RNA; Ctrl, control; siRNA, small interference RNA; GAPDH, glyceraldehyde-3-phosphate dehydrogenase.

role in EOC progression and that knockdown of SphK2 could significantly inhibit the proliferation of cancer. Especially, our study provided the following new findings: (I) SphK2, up-regulated in ovarian cancer tissues, correlated with a poor prognosis in this deadly disease; (II) SphK2 blockage in EOC cells caused significant inhibition of cell growth and an arrest in the G1/G0 phase; (III) inhibition of SphK2 down-regulated ERK/c-Myc pathway, which might partly mediate SphK2 induced cell cycle arrest.

The SphKs exhibit 2 isoforms, SphK1 and SphK2. A key player in cancer progression, SphK1 (31), is elevated markedly in ovarian cancer (13,32). Our previous studies showed SphK1 was required for EOC metastasis and angiogenesis (12,13), and its activation inversely correlated with survival in EOC patients (20). Moreover, it is reported that S1P, generated by SphK, was elevated in ascites of ovarian cancer patients (33) and was also reported to regulate the migration, invasion, and angiogenesis of ovarian cancer cells. However, the expression and function of SphK2 are far from elucidated (33,34). Here, we showed that the level of SphK2 was elevated in EOC specimens. Notably, the SphK2 level was closely correlated with the well-known prognostic parameters of EOC, including FIGO stage, histological grade, lymph node metastasis, and ascites.

Moreover, the elevated expression level of SphK2 was found to be associated with poor prognosis and was a prognostic factor for predicting OS and RFS. These findings implied that SphK2 might be a potentially important factor in EOC progression. Beach et al. reported that SphK2 mRNA was not overexpressed in serous ovarian cancer than normal ovarian tissue (35). However, their study did not distinguish the expression level of SphK2 between ovarian epithelial tissue and adjacent stroma. Therefore, further studies are needed to detect the SphK2 expression quantities of normal ovary epithelial tissue and EOC tissue. Moreover, SphK1 was reported to be highly expressed in tumor stroma and was required for the differentiation and tumor-promoting function of cancer-associated fibroblasts (35). However, the roles of SphK2 in cells of the tumor stroma remain unclear and require exploration in the future.

The contribution of SphK2 to cancer progression is unclear. Some studies have found that high-level expression of SphK2 could induce cell cycle arrest and apoptosis (14,15). Despite the notion that SphK2 is a pro-apoptotic factor, several studies have emerged indicating SphK2 promoted cancer survival. Knockdown or inhibition of SphK2 has been shown to induce apoptosis in some

cancer types (16,17). Moreover, in some cancer cell lines, targeting SphK2 has an even more powerful anti-cancer effect than targeting SphK1 (36,37). In this study, the relationship between SphK2 levels and EOC patients' prognosis suggests a role for SphK2 in promoting EOC. Therefore, we investigated the effect of SphK2 down-regulation on the growth of EOC cells *in vitro*. As expected, SphK2 blockage by shRNA significantly inhibited ovarian cancer proliferation. Following the *in vitro* results, SphK2 down-regulation also reduced tumor growth in a mouse ovarian cancer model. These results indicated that SphK2 was associated with EOC progression and presented the possibility that SphK2 might serve as a new target for EOC therapy. In future studies, more EOC cell lines and primary EOC cells should be tested further to verify the role of SphK2 in EOC progression.

Inhibition of SphK2 has been reported to be associated with both caspase-dependent and autophagy-dependent cell death (17,38). In ovarian cancer, SphK2 down-regulated cells displayed only modest levels of early and late apoptotic cells. Consistent with the lack of apoptosis, genes involved in apoptosis were not changed significantly in SphK2 down-regulated cells (data not shown). In contrast to the modest effects in cell apoptosis, SphK2 depleted cells showed a dramatic accumulation in the G0/G1 phase compared to the controls. Moreover, SphK2 down-regulation caused cyclin D1 and phosphor-Rb inhibition, several key cell cycle checkpoint factors.

Furthermore, autophagy is implicated in both cell death and cell survival. The potential regulation of autophagy by SphK2 and its roles in EOC growth need to be investigated in a future study. Taken together, our data indicated that the primary cellular mechanism, whereby inhibition of SphK2 prevented cell growth of ovarian cancer cells, is mediated through the inhibition of cell cycle progression rather than induction of apoptosis.

Another new finding in this study was the down-regulation of the ERK/c-Myc pathway due to SphK2 inhibition. Our results are consistent with previous studies demonstrating that SphK2 inhibition down-regulated c-Myc expression (21,39). Extensive studies have demonstrated the essential roles of ERK1/2 signaling in ovarian cancer survival (40-42). Moreover, c-Myc, an inducible ERK gene, was reported to be a key mediator of the progression of ovarian cancer (43,44). Furthermore, ERK or c-Myc inhibition has been reported to cause a G0/G1 block in the cell cycle of ovarian cancer cells (40,43). Therefore, it is possible that inhibition of SphK2 resulted in the repression

of the ERK/c-Myc pathway and subsequently caused G0/G1 cell cycle arrest, which consequently reduced cell proliferation in human EOC.

Moreover, it was reported that ERK1 could activate SphK2 by direct phosphorylation in breast cancer (45), which indicated that ERK1 was the upstream activator of SphK2. This report, together with our observation that SphK2 blockage resulted in significant ERK activation inhibition, suggests ERK1 might be placed in both upstream and downstream of SphK2 signaling and might have a dual role in the initiation and amplification of the SphK2 signaling loop in EOC cells. This speculation needs to be further investigated in the future. Besides, the biological effects of SphK2 activation chiefly rely on its product S1P. Therefore, further studies are needed to explore the functions of extracellular and intracellular S1P generated by SphK2. Furthermore, the connection between SphK2 and ERK/c-Myc pathway needs to be further validated in tumor tissue sections.

Acknowledgments

Funding: This study was supported by the grants from the National Natural Science Foundation of China (NSFC) (81974401 to Lan Dai, and 81772770 to Wen Di), the Science and Technology Commission of Shanghai municipality (18ZR1423100 to Lan Dai), and the Shanghai Municipal Commission of Health and Family Planning (2017YQ035 to Lan Dai).

Footnote

Reporting Checklist: The authors have completed the ARRIVE reporting checklist. Available at <http://dx.doi.org/10.21037/atm-20-6742>

Data Sharing Statement: Available at <http://dx.doi.org/10.21037/atm-20-6742>

Conflicts of Interest: All authors have completed the ICMJE uniform disclosure form (available at <http://dx.doi.org/10.21037/atm-20-6742>). The authors have no conflicts of interest to declare.

Ethical Statement: The authors are accountable for all aspects of the work in ensuring that questions related to the accuracy or integrity of any part of the work are appropriately investigated and resolved. All animal

experiments were performed according to the Laboratory Animal Guidelines provided by Shanghai Jiao Tong University School of Medicine. The experimental protocols were approved by the Institutional Animal Care and Use Committee of Shanghai Jiao Tong University School of Medicine (A2018021). All procedures performed in this study involving human participants were in accordance with the Declaration of Helsinki (as revised in 2013). The study was approved by the Institutional Ethical Committee of Renji Hospital (RA-2019-076) and informed consent was provided by all participants.

Open Access Statement: This is an Open Access article distributed in accordance with the Creative Commons Attribution-NonCommercial-NoDerivs 4.0 International License (CC BY-NC-ND 4.0), which permits the non-commercial replication and distribution of the article with the strict proviso that no changes or edits are made and the original work is properly cited (including links to both the formal publication through the relevant DOI and the license). See: <https://creativecommons.org/licenses/by-nc-nd/4.0/>.

References

1. Siegel RL, Miller KD, Jemal A. Cancer statistics, 2019. *CA Cancer J Clin* 2019;69:7-34.
2. Bowtell DD, Bohm S, Ahmed AA, et al. Rethinking ovarian cancer II: reducing mortality from high-grade serous ovarian cancer. *Nat Rev Cancer* 2015;15:668-79.
3. Agarwal R, Kaye SB. Ovarian cancer: strategies for overcoming resistance to chemotherapy. *Nat Rev Cancer* 2003;3:502-16.
4. Schwartz M, Camacho-Vanegas O, Wood AM, et al. Applying Precision Medicine to Ovarian Cancer: Proof-of-Principle for a "Molecular Second Look". *Int J Gynecol Cancer* 2018;28:479-85.
5. Yap TA, Carden CP, Kaye SB. Beyond chemotherapy: targeted therapies in ovarian cancer. *Nat Rev Cancer* 2009;9:167-81.
6. Ogretmen B. Sphingolipid metabolism in cancer signalling and therapy. *Nat Rev Cancer* 2018;18:33-50.
7. Takabe K, Paugh SW, Milstien S, et al. "Inside-out" signaling of sphingosine-1-phosphate: therapeutic targets. *Pharmacol Rev* 2008;60:181-95.
8. Dai L, Xia P, Di W. Sphingosine 1-phosphate: a potential molecular target for ovarian cancer therapy? *Cancer Invest* 2014;32:71-80.
9. Acharya S, Yao J, Li P, et al. Sphingosine Kinase 1

- Signaling Promotes Metastasis of Triple-Negative Breast Cancer. *Cancer Res* 2019;79:4211-26.
10. Lee CF, Dang A, Hernandez E, et al. Activation of sphingosine kinase by lipopolysaccharide promotes prostate cancer cell invasion and metastasis via SphK1/S1PR4/matriptase. *Oncogene* 2019;38:5580-98.
 11. Hart PC, Chiyoda T, Liu X, et al. SPHK1 Is a Novel Target of Metformin in Ovarian Cancer. *Mol Cancer Res* 2019;17:870-81.
 12. Dai L, Liu Y, Xie L, et al. Sphingosine kinase 1/sphingosine-1-phosphate (S1P)/S1P receptor axis is involved in ovarian cancer angiogenesis. *Oncotarget* 2017;8:74947-61.
 13. Zhang H, Wang Q, Zhao Q, et al. MiR-124 inhibits the migration and invasion of ovarian cancer cells by targeting SphK1. *J Ovarian Res* 2013;6:84.
 14. Maceyka M, Sankala H, Hait NC, et al. SphK1 and SphK2, sphingosine kinase isoenzymes with opposing functions in sphingolipid metabolism. *J Biol Chem* 2005;280:37118-29.
 15. Liu H, Toman RE, Goparaju SK, et al. Sphingosine kinase type 2 is a putative BH3-only protein that induces apoptosis. *J Biol Chem* 2003;278:40330-6.
 16. Liang J, Zhang X, He S, et al. Sphk2 RNAi nanoparticles suppress tumor growth via downregulating cancer cell derived exosomal microRNA. *J Control Release* 2018;286:348-57.
 17. Dai L, Smith CD, Foroozesh M, et al. The sphingosine kinase 2 inhibitor ABC294640 displays anti-non-small cell lung cancer activities in vitro and in vivo. *Int J Cancer* 2018;142:2153-62.
 18. Neubauer HA, Pham DH, Zebol JR, et al. An oncogenic role for sphingosine kinase 2. *Oncotarget* 2016;7:64886-99.
 19. Chen Y, Deng X, Chen W, et al. Silencing of microRNA-708 promotes cell growth and epithelial-to-mesenchymal transition by activating the SPHK2/AKT/beta-catenin pathway in glioma. *Cell Death Dis* 2019;10:448.
 20. Song K, Dai L, Long X, et al. Follicle-stimulating hormone promotes the proliferation of epithelial ovarian cancer cells by activating sphingosine kinase. *Sci Rep* 2020;10:13834.
 21. Wallington-Beddoe CT, Powell JA, Tong D, et al. Sphingosine kinase 2 promotes acute lymphoblastic leukemia by enhancing MYC expression. *Cancer Res* 2014;74:2803-15.
 22. Song K, Dai L, Long X, et al. Sphingosine kinase 2 inhibitor ABC294640 displays anti-epithelial ovarian cancer activities in vitro and in vivo. *Onco Targets Ther* 2019;12:4437-49.
 23. Dai L, Qi Y, Chen J, et al. Sphingosine kinase (SphK) 1 and SphK2 play equivalent roles in mediating insulin's mitogenic action. *Mol Endocrinol* 2014;28:197-207.
 24. Dai L, Gu L, Ding C, et al. TWEAK promotes ovarian cancer cell metastasis via NF-kappaB pathway activation and VEGF expression. *Cancer Lett* 2009;283:159-67.
 25. Wang Y, Wang Y, Xiang J, et al. Knockdown of CRM1 inhibits the nuclear export of p27(Kip1) phosphorylated at serine 10 and plays a role in the pathogenesis of epithelial ovarian cancer. *Cancer Lett* 2014;343:6-13.
 26. Deng W, Wang Y, Liu Z, et al. HemI: a toolkit for illustrating heatmaps. *PLoS One* 2014;9:e111988.
 27. Chang F, Steelman LS, Shelton JG, et al. Regulation of cell cycle progression and apoptosis by the Ras/Raf/MEK/ERK pathway (Review). *Int J Oncol* 2003;22:469-80.
 28. Junttila MR, Westermarck J. Mechanisms of MYC stabilization in human malignancies. *Cell Cycle* 2008;7:592-6.
 29. Pelengaris S, Khan M. The c-MYC oncoprotein as a treatment target in cancer and other disorders of cell growth. *Expert Opin Ther Targets* 2003;7:623-42.
 30. Sears R, Nuckolls F, Haura E, et al. Multiple Ras-dependent phosphorylation pathways regulate Myc protein stability. *Genes Dev* 2000;14:2501-14.
 31. Zheng X, Li W, Ren L, et al. The sphingosine kinase-1/sphingosine-1-phosphate axis in cancer: Potential target for anticancer therapy. *Pharmacol Ther* 2019;195:85-99.
 32. Yang YL, Ji C, Cheng L, et al. Sphingosine kinase-1 inhibition sensitizes curcumin-induced growth inhibition and apoptosis in ovarian cancer cells. *Cancer Sci* 2012;103:1538-45.
 33. Wang D, Zhao Z, Caperell-Grant A, et al. S1P differentially regulates migration of human ovarian cancer and human ovarian surface epithelial cells. *Mol Cancer Ther* 2008;7:1993-2002.
 34. Park KS, Kim MK, Lee HY, et al. S1P stimulates chemotactic migration and invasion in OVCAR3 ovarian cancer cells. *Biochem Biophys Res Commun* 2007;356:239-44.
 35. Beach JA, Aspuria PJ, Cheon DJ, et al. Sphingosine kinase 1 is required for TGF-beta mediated fibroblast-to-myofibroblast differentiation in ovarian cancer. *J Neuropathol Exp Neurol* 2005;64:695-705.
 36. Van Brocklyn JR, Jackson CA, Pearl DK, et al. Sphingosine kinase-1 expression correlates with poor

- survival of patients with glioblastoma multiforme: roles of sphingosine kinase isoforms in growth of glioblastoma cell lines. *J Neuropathol Exp Neurol* 2005; 64:695-705.
37. Gao P, Smith CD. Ablation of sphingosine kinase-2 inhibits tumor cell proliferation and migration. *Mol Cancer Res* 2011;9:1509-19.
 38. Dai L, Bai A, Smith CD, et al. ABC294640, A Novel Sphingosine Kinase 2 Inhibitor, Induces Oncogenic Virus-Infected Cell Autophagic Death and Represses Tumor Growth. *Mol Cancer Ther* 2017;16:2724-34.
 39. Venkata JK, An N, Stuart R, et al. Inhibition of sphingosine kinase 2 downregulates the expression of c-Myc and Mcl-1 and induces apoptosis in multiple myeloma. *Blood* 2014;124:1915-25.
 40. Jiang XL, Gao JC, Jiang L, et al. Expression and significance of MAPK/ERK in the specimens and cells of epithelial ovarian cancer. *Zhonghua Fu Chan Ke Za Zhi* 2019;54:541-7.
 41. Liu SB, Lin XP, Xu Y, et al. DAXX promotes ovarian cancer ascites cell proliferation and migration by activating the ERK signaling pathway. *J Ovarian Res* 2018;11:90.
 42. Liu S, Zha J, Lei M. Inhibiting ERK/Mnk/eIF4E broadly sensitizes ovarian cancer response to chemotherapy. *Clin Transl Oncol* 2018;20:374-81.
 43. Reyes-Gonzalez JM, Armaiz-Pena GN, Mangala LS, et al. Targeting c-MYC in Platinum-Resistant Ovarian Cancer. *Mol Cancer Ther* 2015;14:2260-9.
 44. Zeng M, Kwiatkowski NP, Zhang T, et al. Targeting MYC dependency in ovarian cancer through inhibition of CDK7 and CDK12/13. *Elife* 2018;7:e39030.
 45. Hait NC, Bellamy A, Milstien S, et al. Sphingosine kinase type 2 activation by ERK-mediated phosphorylation. *J Biol Chem* 2007;282:12058-65.

Cite this article as: Dai L, Wang W, Liu Y, Song K, Di W. Inhibition of sphingosine kinase 2 down-regulates ERK/c-Myc pathway and reduces cell proliferation in human epithelial ovarian cancer. *Ann Transl Med* 2021;9(8):645. doi: 10.21037/atm-20-6742

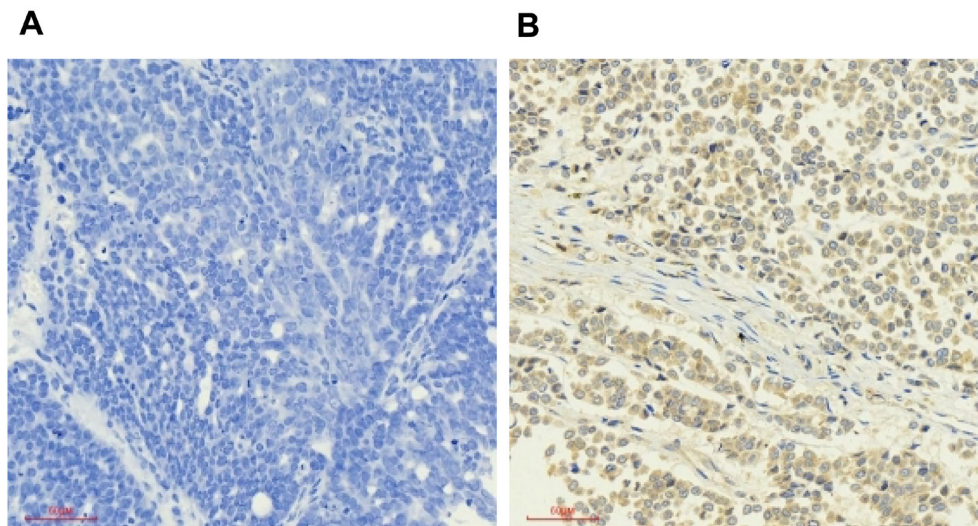


Figure S1 The negative and positive control of IHC. (A) Negative control: IHC staining of serous ovarian cancer tissue. Normal rabbit immunoglobulins were used as primary antibodies. (B) Positive control: IHC staining of SphK2 in human breast cancer tissue. The scale bar represents 60 μm . IHC, immunohistochemistry.

Table S1 100 most significant changed genes of SKOV3 cells transfected with SphK2 shRNA

GeneSymbol	Normalized signal (log2) of NC1	Normalized signal (log2) of NC2	Normalized signal (log2) of NC3	Normalized signal (log2) of SphK2-1	Normalized signal (log2) of SphK2-2	Normalized signal (log2) of SphK2-3	Gene_ID	Accession
<i>CAPN13</i>	1.723441	1.821052	1.618743	6.354988	6.531311	6.218926	92291	AK074418
<i>STON1-GTF2A1L</i>	1.663951	1.801454	1.463038	6.213173	6.139173	6.350677	286749	NM_172311
<i>TMEM169</i>	1.699259	1.836763	1.769648	6.167417	6.093417	6.304921	92691	NM_138390
<i>SERPINA7</i>	1.658265	1.506262	1.457353	6.122579	6.23361	6.002284	6906	NM_000354
<i>FAM189A2</i>	1.962786	1.826724	2.060397	6.226503	6.137235	6.152502	9413	NM_004816
<i>OR2F1</i>	2.702354	2.903988	2.865853	6.808706	6.933034	6.906317	26211	NM_012369
<i>CRHR1</i>	1.984403	2.121907	1.879706	6.081669	5.992402	6.1927	1394	NM_004382
<i>CXCR2</i>	2.808716	2.946219	2.906327	6.876749	6.787482	6.98778	3579	NM_001557
<i>PLIN5</i>	1.710634	1.605937	1.59034	5.689104	5.584406	5.63021	440503	NM_001013706
<i>LHCGR</i>	1.621096	1.436671	1.452973	5.595267	5.506	5.536373	3973	NM_000233
<i>LRRC55</i>	1.689812	1.853311	1.600545	5.655633	5.779961	5.596739	219527	NM_001005210
<i>SPOCK2</i>	1.925069	2.062572	1.724156	5.848576	5.959607	5.98608	9806	NM_014767
<i>UGT3A1</i>	1.622032	1.548031	1.517334	5.456356	5.526745	5.593859	133688	NM_152404
<i>AXDND1</i>	2.172279	2.26989	2.242669	5.927011	5.806717	6.064515	126859	NM_144696
<i>DCAF12L1</i>	1.735571	1.873074	1.833181	5.389985	5.300718	5.501017	139170	NM_178470
<i>WDTC1</i>	1.791825	1.717825	1.687128	5.423995	5.494385	5.349995	23038	NM_015023
<i>PSD</i>	1.91226	2.009871	1.791966	5.438491	5.333794	5.575995	5662	NM_002779
<i>KRT17P5</i>	1.669043	1.484619	1.500921	5.160319	5.071052	5.25793	339240	NR_001443
<i>Inc-C14orf28-1</i>	1.686466	1.502042	1.518344	5.157382	5.068115	5.098488	Inc-C14orf28-1:3	
<i>MYOT</i>	1.798899	1.597987	1.709632	5.208702	5.33303	5.306313	9499	NM_006790
<i>CHRNA7</i>	3.026047	3.16355	2.921349	6.407561	6.318293	6.271499	1146	NM_005199
<i>RP1L1</i>	3.26524	3.113236	3.349304	6.599514	6.494816	6.479219	94137	NM_178857
<i>ZNF665</i>	2.859678	2.930067	2.75498	6.158239	6.228628	6.084238	79788	NM_024733
<i>GPR6</i>	1.879664	2.003992	1.711542	5.134558	5.191142	5.232169	2830	NM_005284
<i>PPP2R2B</i>	1.959794	1.855097	1.8395	5.212759	5.108062	5.350263	5521	NM_001271948
<i>COL19A1</i>	1.859919	1.997422	1.755221	5.084918	4.99565	4.948856	1310	NM_001858
<i>PPP1R3C</i>	1.831188	1.72649	1.710894	5.012698	4.908001	5.150202	5507	NM_005398
<i>SLC6A2</i>	1.822543	1.67054	1.62163	4.999193	5.110224	5.136697	6530	NM_001043
<i>KCNG4</i>	1.9361	2.060428	1.767977	5.055805	4.966538	5.153416	93107	NM_172347
<i>ZNF558</i>	2.949439	3.019828	2.844741	6.05615	6.126539	5.982149	148156	AK055494
<i>RPS4Y2</i>	1.724131	1.572128	1.808195	4.777621	4.888652	4.657327	140032	NM_001039567
<i>PRY2</i>	1.673558	1.771169	1.553264	4.721532	4.616835	4.859036	442862	NM_001002758
<i>TPMT</i>	1.6696	1.5956	1.73999	4.668473	4.594472	4.805976	7172	NM_000367
<i>ATP10B</i>	3.802994	3.900605	3.873383	6.787623	6.667328	6.925126	23120	NM_025153

Table S1 (continued)

Table S1 (continued)

GeneSymbol	Normalized signal (log2) of NC1	Normalized signal (log2) of NC2	Normalized signal (log2) of NC3	Normalized signal (log2) of SphK2-1	Normalized signal (log2) of SphK2-2	Normalized signal (log2) of SphK2-3	Gene_ID	Accession
<i>LINC00977</i>	1.753568	1.569143	1.585445	4.737893	4.648626	4.678999	728724	NR_033916
<i>CALCA</i>	2.448535	2.546146	2.343838	5.431335	5.607658	5.295273	796	NM_001033952
<i>GRM3</i>	1.720528	1.844856	1.552405	4.693338	4.749921	4.790949	2913	NM_000840
<i>DHRS4-AS1</i>	6.203654	6.341158	6.301265	9.17191	9.082642	9.282941	55449	NR_023921
<i>MMRN2</i>	2.360667	2.524166	2.2714	5.310428	5.434756	5.408039	79812	NM_024756
<i>TMEM229B</i>	1.886745	2.024249	1.957134	4.805802	4.731801	4.943305	161145	XR_245666
<i>Inc-WDR7-6</i>	2.97997	3.143469	3.13053	5.881037	5.79177	5.822144	Inc-WDR7-6:1	
<i>HS3ST3B1</i>	1.925637	2.049965	1.757514	4.753639	4.664371	4.85125	9953	NM_006041
<i>KANK3</i>	2.119384	2.243712	1.951261	4.915372	4.826104	5.012982	256949	NM_198471
<i>IL3</i>	1.795209	1.919537	1.627086	4.570705	4.481438	4.668316	3562	NM_000588
<i>LOC102724794</i>	2.389774	2.553272	2.540333	5.144572	5.2689	5.085679	102724794	BC009926
<i>CYP26A1</i>	1.758812	1.896316	1.856423	4.471999	4.382732	4.583031	1592	NM_057157
<i>GPC3</i>	2.455046	2.579374	2.286923	5.167371	5.223955	5.264982	2719	NM_004484
<i>KIF26A</i>	3.871365	3.68694	3.703242	6.515574	6.426307	6.613185	26153	NM_015656
<i>RSBN1L</i>	5.618802	5.466799	5.702866	8.253452	8.364483	8.133158	222194	BM468849
<i>OR7E47P</i>	1.740766	1.9424	1.904265	4.371512	4.49584	4.469123	26628	NR_120438
<i>KIAA1024L</i>	4.577214	4.39279	4.409092	1.7674	1.678133	1.865011	100127206	NM_001257308
<i>GABRR3</i>	5.933716	6.058045	6.031327	3.114626	3.171209	3.040625	200959	NM_001105580
<i>ATP13A4</i>	4.451427	4.549038	4.521816	1.629519	1.509225	1.767023	84239	NM_032279
<i>CD300LG</i>	5.173277	5.021274	5.06858	2.342911	2.519234	2.20685	146894	NM_145273
<i>MUC15</i>	4.515982	4.315069	4.426715	1.667706	1.792034	1.765317	143662	NM_145650
<i>COBLL1</i>	4.641321	4.778824	4.536623	1.789184	1.699916	1.653122	22837	NM_014900
<i>GPR1-AS</i>	4.620425	4.744753	4.452302	1.738813	1.795397	1.836424	101669764	NR_104359
<i>AIM1L</i>	4.768345	4.865956	4.838735	1.869546	1.749252	1.764849	55057	NM_001039775
<i>EIF1AY</i>	4.597503	4.735006	4.695113	1.692469	1.603202	1.618469	9086	NM_004681
<i>LINC00950</i>	5.974328	5.789904	5.806205	3.066059	2.976792	3.007166	92973	NR_024006
<i>KCNS2</i>	4.556707	4.681035	4.388585	1.643771	1.554503	1.741382	3788	NM_020697
<i>FAM84B</i>	5.05626	4.920198	5.15387	2.12875	2.039483	2.05475	157638	NM_174911
<i>TMEM86A</i>	6.237049	6.374553	6.307438	3.308936	3.234936	3.44644	144110	NM_153347
<i>DCANP1</i>	4.575955	4.713459	4.673566	1.642116	1.552848	1.753147	140947	NM_130848
<i>AVPR1A</i>	4.703392	4.801003	4.773781	1.757399	1.637105	1.894903	140947	NM_130848
<i>LOC643659</i>	4.565467	4.728966	4.4762	1.599728	1.724056	1.540834	643659	AK056971
<i>SPHK2</i>	11.1287	11.2662	10.92778	8.114125	8.225156	8.251628	56848	NM_020126
<i>XLOC_I2_000001</i>	4.821869	4.747869	4.717172	1.806649	1.877038	1.732648	TCONS_I2_00001923	

Table S1 (continued)

Table S1 (continued)

GeneSymbol	Normalized signal (log2) of NC1	Normalized signal (log2) of NC2	Normalized signal (log2) of NC3	Normalized signal (log2) of SphK2-1	Normalized signal (log2) of SphK2-2	Normalized signal (log2) of SphK2-3	Gene_ID	Accession
<i>CACNB2</i>	4.92142	5.01903	4.816722	1.801885	1.978208	1.665823	783	AK128769
<i>AGBL4</i>	4.918867	5.016478	4.989257	1.758832	1.869863	1.654134	84871	AK027348
<i>SZT2</i>	5.466478	5.603982	5.536867	2.260969	2.186968	2.398472	23334	NM_015284
<i>PDE5A</i>	5.870075	5.765377	6.033573	2.64736	2.542663	2.588466	8654	NM_001083
<i>ANO4</i>	5.864137	5.961748	5.934527	2.63483	2.514535	2.530132	121601	NM_178826
<i>TRPV3</i>	4.885111	4.81111	4.9555	1.649519	1.575518	1.787022	162514	NM_145068
<i>CTNND2</i>	4.930207	5.06771	4.825509	1.650221	1.560953	1.761252	1501	NM_001332
<i>LOC100505915</i>	5.401384	5.564882	5.551943	2.083278	1.994011	2.024384	100505915	NR_125434
<i>LOC101927770</i>	5.182151	5.34565	5.332711	1.862326	1.986654	1.803432	101927770	NR_110051
<i>PSG11</i>	8.099883	8.197494	7.979589	4.453627	4.348929	4.59113	5680	NM_002785
<i>MSR1</i>	5.382703	5.546202	5.293436	1.729903	1.854232	1.827514	4481	NM_138715
<i>LOC101929172</i>	6.799461	6.96296	6.950021	3.145706	3.270034	3.086812	101929172	NR_104677
<i>GS1-24F4.2</i>	5.341271	5.465599	5.173148	1.648424	1.705008	1.746035	100652791	NR_045217
<i>SYTL1</i>	5.372369	5.509873	5.442759	1.668484	1.594483	1.805987	84958	NM_032872
<i>LOC100131541</i>	5.566218	5.729717	5.716778	1.808116	1.718849	1.749222	100131541	AY358248
<i>SLC7A14</i>	5.420327	5.268324	5.219414	1.649379	1.76041	1.786882	57709	NM_020949
<i>SLC16A12</i>	6.502291	6.350288	6.301378	2.689233	2.800265	2.568939	387700	NM_213606
<i>ENAM</i>	5.457047	5.594551	5.554658	1.617998	1.52873	1.543997	10117	NM_031889
<i>EHD3</i>	5.696453	5.833956	5.794064	1.709446	1.620179	1.635446	30845	NM_014600
<i>PON1</i>	5.733017	5.628319	5.612722	1.70984	1.605143	1.847344	5444	NM_000446
<i>LOC284412</i>	5.739756	5.903255	5.890316	1.705748	1.830076	1.646855	284412	NR_029390
<i>Inc-ARFGEF2-2</i>	5.854138	5.669713	5.686015	1.678698	1.589431	1.619804	-	AK126019
<i>C21orf62</i>	5.925917	6.023528	5.996307	1.745434	1.921757	1.609373	56245	NM_019596
<i>SLC9C2</i>	6.592031	6.440028	6.391118	2.364139	2.47517	2.501642	284525	NM_178527
<i>Inc-PRMT8-2</i>	5.965704	6.129202	6.116263	1.730351	1.641084	1.671458	-	BX096603
<i>CKM</i>	5.93621	6.073713	5.831512	1.698426	1.609159	1.562365	1158	NM_001824
<i>ZNF729</i>	6.886741	6.95713	6.782043	2.459713	2.530103	2.385713	100287226	NM_001242680
<i>OR51A7</i>	6.135948	6.337582	6.299447	1.651183	1.775511	1.748794	119687	NM_001004749
<i>NBEAL2</i>	6.147131	5.946218	6.057864	1.643982	1.76831	1.741593	23218	NM_015175
<i>OPRM1</i>	6.384385	6.586019	6.547884	1.753117	1.877445	1.850728	4988	NM_000914
<i>SCGB1D2</i>	6.390669	6.238666	6.474733	1.601543	1.712574	1.481249	10647	NM_006551
<i>LNX1</i>	6.436681	6.600179	6.58724	1.602565	1.513298	1.543671	84708	NM_032622

SphK2, sphingosine kinase 2; shRNA, short hairpin RNA; NC, negative control; ID, identification.

Table S2 HALLMARK_MYC_TARGETS_V1 (GSEA details)

Name	Probe	Rank metric score	Running ES	Core enrichment
row_0	UBA2	0.75295496	-0.051006	No
row_1	SMARCC1	0.441985309	-0.100376	No
row_2	SNRPD1	0.38816756	-0.111042	No
row_3	HNRNPU	0.275371343	-0.1672	No
row_4	MRPS18B	0.232058719	-0.192292	No
row_5	MYC	0.22204265	-0.195249	No
row_6	RRM1	0.207781792	-0.203505	No
row_7	TUFM	0.141880929	-0.272709	No
row_8	HNRNPA1	0.139995366	-0.271861	No
row_9	CCT2	0.138858914	-0.269999	No
row_10	UBE2L3	0.135779649	-0.270392	No
row_11	XRCC6	0.134474739	-0.268882	No
row_12	TOMM70A	0.134389117	-0.265936	No
row_13	NHP2	0.132905856	-0.264562	No
row_14	RANBP1	0.132039443	-0.262614	No
row_15	AP3S1	0.130847111	-0.260744	No
row_16	TRIM28	0.127579734	-0.261233	No
row_17	GSPT1	0.125280172	-0.261529	No
row_18	PSMA6	0.123724453	-0.260324	No
row_19	PSMD8	0.119761556	-0.261892	No
row_20	POLE3	0.109567322	-0.270549	No
row_21	IMPDH2	0.1076736	-0.271015	No
row_22	NCBP2	0.107079968	-0.269313	No
row_23	PSMA2	0.106365785	-0.267528	No
row_24	CAD	0.104962997	-0.26677	No
row_25	CCNA2	0.103091829	-0.266601	No
row_26	XPO1	0.102699079	-0.264408	No
row_27	HNRNPD	0.101317599	-0.263239	No
row_28	RPL22	0.100557022	-0.261345	No
row_29	H2AFZ	0.09926755	-0.260622	No
row_30	YWHAQ	0.085262917	-0.276851	No
row_31	PRPF31	0.075119957	-0.289997	No
row_32	GNB2L1	0.06710469	-0.299911	No
row_33	SNRPA1	0.063945368	-0.302707	No
row_34	HNRNPC	0.056119565	-0.312088	No

Table S2 (continued)

Table S2 (continued)

Name	Probe	Rank metric score	Running ES	Core enrichment
row_35	RPS5	0.055559836	-0.311363	No
row_36	PSMD7	0.05439749	-0.311359	No
row_37	RPL34	0.052501261	-0.312691	No
row_38	XPOT	0.052221946	-0.311896	No
row_39	CLNS1A	0.052013975	-0.310858	No
row_40	PCNA	0.045902282	-0.317307	No
row_41	NDUFAB1	0.045787055	-0.316318	No
row_42	NOLC1	0.045039382	-0.31619	No
row_43	IFRD1	0.044070806	-0.316432	No
row_44	IARS	0.036820859	-0.324833	No
row_45	SNRPB2	0.03491557	-0.326434	No
row_46	NME1	0.028353699	-0.33459	No
row_47	PSMB2	0.026027661	-0.337444	No
row_48	HSPD1	0.025041765	-0.338585	No
row_49	HNRNPA3	0.025041739	-0.33799	No
row_50	GNL3	0.024733359	-0.337799	No
row_51	MRPL23	0.020495223	-0.341876	No
row_52	MCM7	0.020237211	-0.341841	No
row_53	RAN	0.019865079	-0.342163	No
row_54	HSPE1	0.017159631	-0.345128	No
row_55	CDK4	0.015760908	-0.346886	No
row_56	PSMA1	0.015633628	-0.346763	No
row_57	PPM1G	0.014878112	-0.347203	No
row_58	RPLP0	0.013469636	-0.348619	No
row_59	CSTF2	0.009877304	-0.353246	No
row_60	PSMD14	0.00620796	-0.357513	No
row_61	RPL14	0.004616383	-0.359437	No
row_62	PPIA	0.002007276	-0.362763	No
row_63	SRSF2	-0.014217941	-0.385741	No
row_64	PGK1	-0.018825812	-0.391197	No
row_65	RPL18	-0.019023182	-0.390893	No
row_66	RPS3	-0.021245448	-0.392819	No
row_67	RSL1D1	-0.021759583	-0.393244	No
row_68	RPS10	-0.026557757	-0.399012	No
row_69	PSMC4	-0.03433685	-0.408912	No

Table S2 (continued)

Table S2 (continued)

Name	Probe	Rank metric score	Running ES	Core enrichment
row_70	HDGF	-0.035441697	-0.409905	No
row_71	PSMA7	-0.035912897	-0.409597	No
row_72	FBL	-0.035930786	-0.408792	No
row_73	HPRT1	-0.037053823	-0.4093	No
row_74	TRA2B	-0.039255165	-0.410996	No
row_75	RRP9	-0.040565018	-0.411917	No
row_76	UBE2E1	-0.040684555	-0.411198	No
row_77	LSM2	-0.054305311	-0.428956	No
row_78	CDK2	-0.054875091	-0.428247	No
row_79	TXNL4A	-0.065190256	-0.44029	No
row_80	GLO1	-0.065689772	-0.439225	No
row_81	TFDP1	-0.067489475	-0.439505	No
row_82	VBP1	-0.072169319	-0.443147	No
row_83	C1QBP	-0.078820862	-0.450054	No
row_84	PTGES3	-0.083282806	-0.453829	No
row_85	LSM7	-0.084112555	-0.452673	No
row_86	SSBP1	-0.084295653	-0.450768	No
row_87	EPRS	-0.085567839	-0.450421	No
row_88	TCP1	-0.11050456	-0.476567	No
row_89	SNRPG	-0.115020134	-0.478992	No
row_90	COPS5	-0.11821723	-0.480051	No
row_91	APEX1	-0.11884474	-0.477722	No
row_92	RPL6	-0.122988902	-0.479511	No
row_93	YWHAE	-0.124661528	-0.477787	No
row_94	DDX18	-0.130250916	-0.48119	No
row_95	GOT2	-0.131161422	-0.478965	No
row_96	HDDC2	-0.132284909	-0.476663	No
row_97	SRPK1	-0.146622136	-0.487118	Yes
row_98	NOP56	-0.148529723	-0.485174	Yes
row_99	EIF4G2	-0.149976537	-0.483048	Yes
row_100	RUVBL2	-0.151623368	-0.481428	Yes
row_101	FAM120A	-0.157058418	-0.483201	Yes
row_102	DHX15	-0.160647944	-0.482954	Yes
row_103	ODC1	-0.161853611	-0.480693	Yes
row_104	PSMC6	-0.163321689	-0.478398	Yes

Table S2 (continued)

Table S2 (continued)

Name	Probe	Rank metric score	Running ES	Core enrichment
row_105	VDAC3	-0.169090107	-0.479786	Yes
row_106	SSB	-0.171148852	-0.477751	Yes
row_107	EIF2S1	-0.17292048	-0.475575	Yes
row_108	PSMD3	-0.174922407	-0.473947	Yes
row_109	MCM6	-0.177651942	-0.472552	Yes
row_110	CBX3	-0.178819522	-0.469194	Yes
row_111	PWP1	-0.183310106	-0.468705	Yes
row_112	ORC2	-0.192079425	-0.471382	Yes
row_113	HNRNPA2B1	-0.193108097	-0.467635	Yes
row_114	SRSF3	-0.19625476	-0.465797	Yes
row_115	KPNA2	-0.19806917	-0.462924	Yes
row_116	EIF2S2	-0.200332135	-0.459501	Yes
row_117	ILF2	-0.204584301	-0.458408	Yes
row_118	SNRPD3	-0.204796284	-0.453738	Yes
row_119	CCT5	-0.20759435	-0.450986	Yes
row_120	RNPS1	-0.209443837	-0.447198	Yes
row_121	MAD2L1	-0.214259252	-0.445924	Yes
row_122	TYMS	-0.215162262	-0.441454	Yes
row_123	POLD2	-0.225046277	-0.442851	Yes
row_124	RPS6	-0.225984603	-0.438471	Yes
row_125	BUB3	-0.228153363	-0.434982	Yes
row_126	STARD7	-0.229092807	-0.430677	Yes
row_127	EEF1B2	-0.231023133	-0.426773	Yes
row_128	DEK	-0.231684506	-0.421662	Yes
row_129	HSP90AB1	-0.232376978	-0.416733	Yes
row_130	PHB2	-0.236070171	-0.413403	Yes
row_131	PSMD1	-0.23623085	-0.408036	Yes
row_132	SYNCRIP	-0.239132211	-0.404583	Yes
row_133	PHB	-0.23959583	-0.399036	Yes
row_134	PSMA4	-0.241566703	-0.394931	Yes
row_135	PRDX3	-0.243438482	-0.39093	Yes
row_136	NAP1L1	-0.243779406	-0.385383	Yes
row_137	TARDBP	-0.245692894	-0.380832	Yes
row_138	SERBP1	-0.248633698	-0.376856	Yes
row_139	U2AF1	-0.25003773	-0.371855	Yes

Table S2 (continued)

Table S2 (continued)

Name	Probe	Rank metric score	Running ES	Core enrichment
row_140	PCBP1	-0.250153869	-0.365908	Yes
row_141	PRPS2	-0.251016259	-0.360437	Yes
row_142	CUL1	-0.25416702	-0.355734	Yes
row_143	NPM1	-0.26072982	-0.353356	Yes
row_144	VDAC1	-0.262458354	-0.347762	Yes
row_145	RFC4	-0.266047537	-0.344067	Yes
row_146	G3BP1	-0.269299239	-0.340244	Yes
row_147	CDC20	-0.273317069	-0.336178	Yes
row_148	NOP16	-0.278643012	-0.333225	Yes
row_149	EXOSC7	-0.280433416	-0.327501	Yes
row_150	EIF3B	-0.281347871	-0.321458	Yes
row_151	MCM5	-0.288626343	-0.319061	Yes
row_152	SET	-0.296802521	-0.316272	Yes
row_153	CNBP	-0.29850772	-0.310218	Yes
row_154	ABCE1	-0.300362378	-0.303921	Yes
row_155	CYC1	-0.306511402	-0.299859	Yes
row_156	USP1	-0.306835771	-0.292614	Yes
row_157	ERH	-0.307143658	-0.285511	Yes
row_158	CDC45	-0.309706509	-0.27934	Yes
row_159	NCBP1	-0.311334372	-0.272931	Yes
row_160	PABPC4	-0.31315735	-0.26628	Yes
row_161	KPNB1	-0.313886315	-0.258818	Yes
row_162	MRPL9	-0.314340293	-0.251693	Yes
row_163	SRSF7	-0.314915717	-0.244753	Yes
row_164	SNRPD2	-0.317407101	-0.238497	Yes
row_165	CCT7	-0.31781745	-0.231091	Yes
row_166	EIF3J	-0.328673124	-0.228635	Yes
row_167	KARS	-0.336773813	-0.225144	Yes
row_168	RPS2	-0.339905143	-0.218006	Yes
row_169	AIMP2	-0.356947273	-0.217111	Yes
row_170	LDHA	-0.361901045	-0.210938	Yes
row_171	CANX	-0.374194205	-0.207053	Yes
row_172	EIF1AX	-0.399766922	-0.206033	Yes
row_173	EIF3D	-0.403767079	-0.197923	Yes
row_174	SLC25A3	-0.413684905	-0.190916	Yes

Table S2 (continued)

Table S2 (continued)

Name	Probe	Rank metric score	Running ES	Core enrichment
row_175	RAD23B	-0.417804658	-0.182225	Yes
row_176	PSMB3	-0.417925298	-0.17229	Yes
row_177	ACP1	-0.424158156	-0.164141	Yes
row_178	PABPC1	-0.424715102	-0.154442	Yes
row_179	HDAC2	-0.438016325	-0.147799	Yes
row_180	CCT4	-0.450546712	-0.140413	Yes
row_181	SF3B3	-0.470833033	-0.134727	Yes
row_182	DDX21	-0.476490498	-0.12459	Yes
row_183	SRM	-0.481136769	-0.114343	Yes
row_184	COX5A	-0.495382637	-0.106932	Yes
row_185	CCT3	-0.516387105	-0.09937	Yes
row_186	ETF1	-0.526386082	-0.089039	Yes
row_187	PA2G4	-0.558176398	-0.081872	Yes
row_188	EIF4E	-0.61265403	-0.076733	Yes
row_189	EIF4A1	-0.617235363	-0.062805	Yes
row_190	MCM2	-0.631449163	-0.050572	Yes
row_191	EIF4H	-0.653316855	-0.038762	Yes
row_192	DUT	-0.661347389	-0.023883	Yes
row_193	PRDX4	-0.684686899	-0.011774	Yes
row_194	SNRPA	-0.703109384	0.0027078	Yes
row_195	SRSF1	-0.735901058	0.0154889	Yes
row_196	MCM4	-0.753878117	0.0311778	Yes
row_197	HNRNPR	-0.772973239	0.0470725	Yes
row_198	SF3A1	-0.793221414	0.0635974	Yes

GSEA, Gene set enrichment analysis; ES, enrichment score.

Table S3 HALLMARK_MYC_TARGETS_V2 (GSEA details)

Name	Probe	Rank metric score	Running ES	Core enrichment
row_0	MYC	0.22204265	-0.23330317	No
row_1	SORD	0.147695452	-0.3013698	No
row_2	MPHOSPH10	0.142654836	-0.29727072	No
row_3	MYBBP1A	0.100131452	-0.34115317	No
row_4	RABEPK	0.076708563	-0.36774597	No
row_5	NOLC1	0.045039382	-0.40718013	No
row_6	WDR74	0.042263422	-0.40828314	No
row_7	HSPD1	0.025041765	-0.42954922	No
row_8	GNL3	0.024733359	-0.42827404	No
row_9	IPO4	0.020873915	-0.43101102	No
row_10	HSPE1	0.017159631	-0.4348436	No
row_11	CDK4	0.015760908	-0.4358668	No
row_12	TMEM97	-0.003955827	-0.46135676	No
row_13	PLK1	-0.005095467	-0.4626284	No
row_14	PPRC1	-0.011475308	-0.47104335	No
row_15	FARSA	-0.031356916	-0.49556538	No
row_16	SLC19A1	-0.038516253	-0.50259405	No
row_17	RRP9	-0.040565018	-0.50258344	No
row_18	NDUFAF4	-0.080790021	-0.54914	No
row_19	TBRG4	-0.100404747	-0.56580997	No
row_20	PPAN	-0.119243138	-0.5789049	No
row_21	DDX18	-0.130250916	-0.5817764	Yes
row_22	IMP4	-0.136173263	-0.5777336	Yes
row_23	UTP20	-0.145401374	-0.57649803	Yes
row_24	NOP56	-0.148529723	-0.5690842	Yes
row_25	RCL1	-0.151270196	-0.56148	Yes
row_26	GRWD1	-0.166755065	-0.56610096	Yes
row_27	RRP12	-0.173035681	-0.5603343	Yes
row_28	NIP7	-0.173853666	-0.5494367	Yes
row_29	MAP3K6	-0.17443873	-0.53790724	Yes
row_30	CBX3	-0.178819522	-0.52971894	Yes
row_31	HK2	-0.197324991	-0.53187096	Yes
row_32	NOP2	-0.198687613	-0.51914924	Yes
row_33	NOC4L	-0.214178205	-0.51658326	Yes
row_34	PHB	-0.23959583	-0.51934516	Yes

Table S3 (continued)

Table S3 (continued)

Name	Probe	Rank metric score	Running ES	Core enrichment
row_35	BYSL	-0.248257443	-0.50884444	Yes
row_36	NPM1	-0.26072982	-0.49777272	Yes
row_37	EXOSC5	-0.26488322	-0.4816831	Yes
row_38	DCTPP1	-0.271444321	-0.46755153	Yes
row_39	NOP16	-0.278643012	-0.45311677	Yes
row_40	PRMT3	-0.280235976	-0.4344825	Yes
row_41	MCM5	-0.288626343	-0.4196497	Yes
row_42	TFB2M	-0.295468986	-0.40266645	Yes
row_43	SUPV3L1	-0.314724982	-0.39104506	Yes
row_44	AIMP2	-0.356947273	-0.38629338	Yes
row_45	TCOF1	-0.368350565	-0.3653299	Yes
row_46	LAS1L	-0.396683842	-0.3479152	Yes
row_47	SRM	-0.481136769	-0.33877108	Yes
row_48	UNG	-0.481530875	-0.30541116	Yes
row_49	PUS1	-0.486822188	-0.27321076	Yes
row_50	WDR43	-0.487907529	-0.23950633	Yes
row_51	MRTO4	-0.540132403	-0.21384856	Yes
row_52	PA2G4	-0.558176398	-0.17846371	Yes
row_53	PES1	-0.568203509	-0.14060867	Yes
row_54	SLC29A2	-0.696943164	-0.113710806	Yes
row_55	PLK4	-0.704164445	-0.06571903	Yes
row_56	MCM4	-0.753878117	-0.020135336	Yes
row_57	DUSP2	-1.268203259	0.031331763	Yes

GSEA, Gene set enrichment analysis; ES, enrichment score.